Available online at www.sciencedirect.com
SCIENCE DIRECT®
Journal of Computational Physics 214 (2006) 264–283
JOURNAL OF COMPUTATIONAL PHYSICS
www.elsevier.com/locate/jcp

From Navier–Stokes to Stokes by means of particle methods

Anthony Beaudoin, Serge Huberson, Elie Rivoalen *

Laboratoire de Mécanique, Physique et Géoscience, Université du Havre, 25 rue Philippe Lebon, BP 540, 76058 Le Havre Cedex, France

Received 27 May 2004; received in revised form 20 September 2005; accepted 20 September 2005
Available online 22 November 2005

Abstract

The viscous flow around a circular cylinder was investigated by means of a particle method over a wide Reynolds number range, from 0.0001 to 1000. A special care was devoted to the satisfaction of the no-slip condition which was expressed through a fourth order partial differential equation for the stream function according to the method initially proposed by Achdou and Pironneau. This equation was solved by a boundary integral method which simultaneously satisfied a Dirichlet and a Neumann condition. The algorithm was immersed within a particle method framework and results in a versatile method which can deal with relatively high Reynolds numbers as well as Stokes flows. The numerical results were analysed and compared to those obtained by others numerically, experimentally and even theoretically for the low Reynolds number limit. The behaviour of the method for the two extreme cases was specially investigated.

1. Introduction

In this paper, we are interested in the simulation of flows with very low Reynolds numbers by means of particle methods. This is not a straightforward application for particle methods which are essentially known to be particularly efficient for the simulation of transport phenomena. However, this is not the only interest of these methods which are also grid-free, thus, well suited to the case of complex or moving boundaries. Our long term objective is to compute flows in porous media at the pore scale for cases where the inertia effects can be of some importance. Therefore, we were looking for a method which can deal with a large range of Reynolds numbers and possibly reproduces an actual Stokes flow. One of our problems was the derivation of proper numerical boundary conditions.

In the boundary integral formulation for the Stokes problem, the normal and tangential boundary conditions are simultaneously solved through the use of the stokelet Green function. Splitting these conditions may still be possible and is actually used for some solution procedures with grid methods. However, this is at the expense of an additional error unless an iterative procedure is used.

* Corresponding author. Tel.: +33 2 32 74 49 76; fax: +33 2 32 74 49 60.
E-mail addresses: Anthony.Beaudoin@univ-lehavre.fr (A. Beaudoin), huberson@univ-lehavre.fr (S. Huberson), rivoalen@univ-lehavre.fr (E. Rivoalen).

0021-9991/$ - see front matter
doi:10.1016/j.jcp.2005.09.014

For two-dimensional flows, it can be argued that the satisfaction of one of the two boundary conditions is sufficient to enforce the no-slip condition. Although this is true for the exact formulation, this solution is not satisfactory for the discrete problem where it corresponds to the reduction of the full matrix of the linear system to its diagonal.

Therefore, it was found desirable to try to solve the two boundary conditions at once: this was the main objective of the work reported hereafter.

The use of particle methods for the simulation of Navier–Stokes flows had to deal with two main difficulties: first, the discretisation of the diffusion differential operator and second, the satisfaction of boundary conditions. These two problems were successfully addressed in Chorin's pioneering work [11] where 2D Navier–Stokes equations for flows around cylinders were solved. Chorin's method made use of two main ingredients: the simulation of diffusion by means of a random walk and the splitting of the no-slip condition into two independent boundary conditions. As a result of this last point, the two conditions arising separately for each component of the velocity were never simultaneously satisfied which was actually the case for the most part of numerical methods for incompressible flows. By the end of the 1980s, that is more than 10 years later, the PSE method was introduced [10,16,19] as an alternative to the random walk.

After further improvements, it turn out that the PSE method was by far preferable to the previous random vortex method (RVM) for many reasons. The first one is the possibility to derive numerical schemes of arbitrary high order [20]. This is an important point since the only way to improve the accuracy of the RVM is to increase the particle numbers and the computational cost accordingly. An other drawback of the RVM is the intrinsic impossibility to combine the method with any re-griding procedure whereas this has been found one of the more efficient way to improve both stability and accuracy of a vortex method [23,15]. A last reason is the difficulty to extend the RVM to three-dimensional flows [21] whereas it is straightforward for the PSE method [15]. These points have been convincingly demonstrated by ample published results [17,35].

However, the satisfaction of boundary conditions still made use of a splitting into separate conditions for the two velocity components. The difficulty was to find a proper boundary integral equation for these conditions since boundary integral methods appeared as the natural tool for works with particle methods. Different alternatives were proposed [24,30,22] all of these using the splitting technique. In the meantime, Chorin himself has brought his first method to a higher degree of sophistication, introducing a specific discretisation for the boundary layer by means of vortex sheets [12]. This last method has been successfully applied to many cases of academic and practical flows in the last 20 years although there are still needs for theoretical works for both accuracy improvements and extension to 3D flows.

The emergence of fast vortex solvers in the last decade enabled particle methods to deal with more realistic geometries and it soon appears that the ability of particle methods to accurately transport a given vorticity field made it a very serious candidate for the simulation of complex separated flows. The basis of particle methods was still more or less the same: a combination of Chorin's boundary conditions splitting and the PSE method. However, decisive improvements were brought and a lot of problems had been solved in order to reach the maturity of today's particle methods. Among the most significant were the works by Koumoutsakos and Leonard [27] who introduced an approximate boundary integral formulation, Cottet and Poncet [17] who used modified smoothing function in the wall region and Winckelmans [34,35] who improved the wall treatment with a very careful account for the vorticity flux at the wall.

Beside this computational effort, the theoretical analysis of particle methods was carried further by mathematicians and proof of convergence was made available for inviscid [4,14] and viscous [5,16,19] unbounded flows. The case of boundary conditions still remained a problem, one reason for that being the difficulty of deriving explicit boundary conditions for vorticity. However, some progress were also made in this direction concerning both formulation [33] and discretisation [32] and new ideas were more recently introduced by Achdou and Pironneau [1,2] and later on by Salvi [37]. In these works, the Navier–Stokes equations rather than the boundary condition itself were split into a diffusion equation and a convective part. Expressing the diffusion equation for the stream function yields a fourth order equation which implies two boundary conditions for both components of the velocity, namely one Dirichlet and one Neumann boundary condition. The homogeneous equation can be expressed as a boundary integral equation which can be solved numerically. The Achdou Pironneau Salvi formulation will be denoted APS formulation hereafter.

In the present work, this method has been implemented within the framework of particle methods. One interesting feature of this method is that it was found to converge to Chorin's original splitting for the case of vanishing viscosity [37]. This point will be checked hereafter, as well as the opposite case of increasing viscosity for which the boundary integral formulation will be shown to converge, at least numerically, to that of a Stokes flow.

2. The APS formulation

Let $\mathscr{D}$ the computational domain, the APS formulation is based on the 2D Navier–Stokes equations expressed in a stream function–vorticity formulation (ψ,ω):

$$\begin{aligned} &\frac{\partial\omega}{\partial t}+\operatorname{div}((\nabla\times\psi)\omega)=\frac{2}{\mathscr{R}_e}\Delta\omega \quad \text{with } \mathscr{R}_e=\frac{DU_\infty}{\nu},\\ &\Delta\psi=-\omega, \end{aligned} \tag{1}$$

together with the boundary conditions on fixed solid walls hereafter denoted $\partial\mathscr{D}$

$$\psi=0 \quad \text{and} \quad \frac{\partial\psi}{\partial\mathbf{n}}=0, \tag{2}$$

where $\mathscr{R}_e$ is the Reynolds number, $R=D/2$ is a characteristic length of the walls, U_∞ is the free-stream velocity, ν denotes the kinematic viscosity, $\partial/\partial\mathbf{n}$ is the normal derivative and $\mathbf{n}$ is the outer normal at the boundary $\partial\mathscr{D}$. The APS formulation aims at concentrating the boundary conditions treatment into one single fourth order equation for the stream function. In order to derive this equation, a two steps procedure was used. The first step consists in a splitting of the vorticity transport equation into a convective and a diffusive part, according to a scheme which has been widely used within the framework of particle methods:

$$\frac{\partial\omega}{\partial t}+\operatorname{div}((\nabla\times\psi)\omega)=0, \tag{3}$$

$$\frac{\partial\omega}{\partial t}-\frac{2}{\mathscr{R}_e}\Delta\omega=0. \tag{4}$$

At each time step, a combination of these two equations was sequentially solved. The resulting scheme was found to approximate the original equation with an error which is proportional to $u\delta t$ to a certain power depending on the time integration scheme used [5].

At this stage, the boundary conditions have not been addressed yet. The first equation is a purely convective equation for the vorticity field and can be easily solved by means of particle methods. The second equation will be further modified. This is the purpose of the second step which consists in the substitution of $\Delta\psi$ for ω in the second equation yielding:

$$\frac{\partial}{\partial t}\Delta\psi-\frac{2}{\mathscr{R}_e}\Delta^2\psi=0. \tag{5}$$

This equation can be solved together with appropriate initial conditions and the boundary conditions (2).

To achieve the goal, Eq. (5) will now be solved. A semi-discrete form was used in order to transform equation (5) into a generalised Helmholtz equation. We first need to discretise the time derivative. Using a crude first order Euler scheme, the following form was obtained at each time step:

$$(\eta\Delta^2-\Delta)\psi^{n+1}=f(\psi^n), \tag{6}$$

where η is a constant equal to $2\delta t/\mathscr{R}_e$ and f a function of ψ computed at the previous time step. The solution of this fourth order elliptic problem can be obtained by using a boundary integral formulation together with the Green function for the 2D generalised Helmholtz problem

$$\mathscr{N}(\mathbf{x})=\frac{1}{2\pi}\left(\log|\mathbf{x}|+K_0\left(\frac{|\mathbf{x}|}{\sqrt{\eta}}\right)\right), \tag{7}$$

where K_0 is the modified Bessel function of the zero kind. Using this Green function and substituting ω^n for $f(\psi^n)$, we get an integral representation for ψ^{n+1}

$$\psi^{n+1}(\mathbf{x}) = \eta \int_{\partial\mathscr{D}} \left(q_2(\mathbf{x}')\mathscr{N}(\mathbf{x}-\mathbf{x}') - q_1(\mathbf{x}')\frac{\partial\mathscr{N}}{\partial\mathbf{n}'}(\mathbf{x}-\mathbf{x}') \right) \mathrm{d}\mathbf{x}' - \int_{\mathscr{D}} \omega^n(\mathbf{x}')\mathscr{N}(\mathbf{x}-\mathbf{x}')\,\mathrm{d}\mathbf{x}'. \tag{8}$$

It can be observed that ψ consists in two parts denoted, respectively, ψ_γ and ψ_ω where:

$$\psi_\gamma^{n+1}(\mathbf{x}) = \eta \int_{\partial\mathscr{D}} \left(q_2(\mathbf{x}')\mathscr{N}(\mathbf{x}-\mathbf{x}') - q_1(\mathbf{x}')\frac{\partial\mathscr{N}}{\partial\mathbf{n}'}(\mathbf{x}-\mathbf{x}') \right) \mathrm{d}\mathbf{x}', \tag{9}$$

$$\psi_\omega^{n+1}(\mathbf{x}) = -\int_{\mathscr{D}} \omega^n(\mathbf{x}')\mathscr{N}(\mathbf{x}-\mathbf{x}')\,\mathrm{d}\mathbf{x}', \tag{10}$$

where q_1 and q_2 are solutions of the following set of boundary integral equations $\forall \mathbf{x} \in \partial\mathscr{D}$:

$$\begin{cases} -\frac{\partial\psi_\omega^{n+1}}{\partial\mathbf{n}}(\mathbf{x}) & = \eta \int_{\partial\mathscr{D}} \left(q_2(\mathbf{x}')\frac{\partial\mathscr{N}}{\partial\mathbf{n}}(\mathbf{x}-\mathbf{x}') - q_1(\mathbf{x}')\frac{\partial^2\mathscr{N}}{\partial\mathbf{n}\partial\mathbf{n}'}(\mathbf{x}-\mathbf{x}') \right) \mathrm{d}\mathbf{x}', \\ -\psi_\omega^{n+1}(\mathbf{x}) & = \eta \int_{\partial\mathscr{D}} \left(q_2(\mathbf{x}')\mathscr{N}(\mathbf{x}-\mathbf{x}') - q_1(\mathbf{x}')\frac{\partial\mathscr{N}}{\partial\mathbf{n}'}(\mathbf{x}-\mathbf{x}') \right) \mathrm{d}\mathbf{x}'. \end{cases} \tag{11}$$

This set of integral equations can be rewritten using a matrix form as

$$\eta\mathscr{A}\mathbf{q} = \mathbf{g} \quad \text{with } \mathscr{A} = \begin{bmatrix} -\frac{\partial^2\mathscr{N}}{\partial\mathbf{n}\partial\mathbf{n}'} & \frac{\partial\mathscr{N}}{\partial\mathbf{n}} \\ -\frac{\partial\mathscr{N}}{\partial\mathbf{n}'} & \mathscr{N} \end{bmatrix}, \quad \mathbf{q} = \begin{bmatrix} q_1 \\ q_2 \end{bmatrix} \quad \text{and} \quad \mathbf{g} = \begin{bmatrix} -\frac{\partial\psi_\omega^{n+1}}{\partial\mathbf{n}} \\ -\psi_\omega^{n+1} \end{bmatrix}. \tag{12}$$

This vorticity is related to the stream function through the Poisson equation

$$\omega = -\Delta\psi, \tag{13}$$

so that it is the solution of the Helmholtz problem:

$$(I - \eta\Delta)\omega^{n+1} = \omega^n. \tag{14}$$

It is worth noting that this is an implicit scheme. This is important since it provides a useful stability property for the Stokes problem solution. An other consequence is the modification of the Green functions to be used which are based on Bessel's functions rather than the usual Gaussian corresponding to a second order diffusion equation. Therefore, the vorticity diffusion computation far from the boundary can be achieved either using the PSE method or a modified PSE in which the Bessel Green function has been substituted to the Gaussian.

An integral representation of ω can be easily derived using the Green function of this last problem which will be denoted $\mathscr{K}^\eta$ hereafter

$$\mathscr{K}^\eta(\mathbf{x}) = \frac{1}{2\pi} K_0\left(\frac{|\mathbf{x}|}{\sqrt{\eta}}\right). \tag{15}$$

We get

$$\omega^{n+1}(\mathbf{x}) = \int_{\partial\mathscr{D}} \left(q_1(\mathbf{x}')\frac{\partial\mathscr{K}^\eta}{\partial\mathbf{n}'}(\mathbf{x}-\mathbf{x}') - q_2(\mathbf{x}')\mathscr{K}^\eta(\mathbf{x}-\mathbf{x}') \right) \mathrm{d}\mathbf{x}' + \frac{1}{\eta}\int_{\mathscr{D}} \omega^n(\mathbf{x}')\mathscr{K}^\eta(\mathbf{x}-\mathbf{x}')\,\mathrm{d}\mathbf{x}'. \tag{16}$$

Taking the curl of the stream function yields the velocity field

$$\mathbf{u}^{n+1}(\mathbf{x}) = \eta \int_{\partial\mathscr{D}} \left(q_2(\mathbf{x}')\mathbf{rot}\mathscr{N}(\mathbf{x}-\mathbf{x}') - q_1(\mathbf{x}')\mathbf{rot}\frac{\partial\mathscr{N}}{\partial\mathbf{n}'}(\mathbf{x}-\mathbf{x}') \right) \mathrm{d}\mathbf{x}' - \int_{\mathscr{D}} \omega^n(\mathbf{x}')\mathbf{rot}\mathscr{N}(\mathbf{x}-\mathbf{x}')\,\mathrm{d}\mathbf{x}'. \tag{17}$$

All these results can be found with more details in [2] or [37].

This is by no mean the only way to solve Eq. (5) together with conditions (2) and other mesh free methods such as the capacitance matrix method [8,31] exist. One interesting feature of the APS formulation is that it provides almost at no additional cost the corresponding vorticity field which is very useful for the coupling with the vortex particle method.

3. Particle discretisation of the APS formulation

In this section, the discretisation of Eqs. (3), (4) and (11) by means of particle methods is considered. We start with the numerical solution of Eq. (11), assuming that ψ_ω is known. The integrals were discretised by using an approximation of $\partial\mathscr{D}$ consisting of a set of small segments $\mathscr{S}_k$. The exact Green function is used and the two terms q_1 and q_2 are approximated by means of piecewise constant functions. On each segment $\mathscr{S}_k$, the constant values of q_1 and q_2 are, respectively, denoted q_1^k and q_2^k. The following approximations for the integrals were used:

$$\int_{\partial\mathscr{D}} q_i(\mathbf{x}')\Phi(\mathbf{x}-\mathbf{x}')\,\mathrm{d}\mathbf{x}' \simeq \sum_k q_i^k \delta l_k \Phi(\mathbf{x}-\mathbf{x}_k) \quad \text{with } i=1,2, \tag{18}$$

where Φ stands for any one of the functions: $\mathscr{N}$, $\partial\mathscr{N}/\partial\mathbf{n}$, $\partial\mathscr{N}/\partial\mathbf{n}'$ and $\partial^2\mathscr{N}/\partial\mathbf{n}\partial\mathbf{n}'$. The length and the middle of the segment $\mathscr{S}_k$ are, respectively, denoted δl_k and $\mathbf{x}_k$. Substituting this discrete form in Eq. (11) yields a set of linear equations for the actualised approximations q_1^k and q_2^k.

We turn now to the vorticity transport equation. Vortex particles were defined by their strength and location denoted, respectively, Ω_i and $\mathbf{x}_i$ for particle $\mathscr{P}_i$. Particle methods are based on the use of Lagrangian coordinates thus the convection equation reduces to the following equation:

$$\frac{\mathrm{d}\chi}{\mathrm{d}t} = \mathbf{u}(\chi,t), \tag{19}$$

where χ is the Lagrangian coordinate which can be substituting by the particle location $\mathbf{x}_i$. The time integration scheme of Eq. (19) which will be used in the calculations is the second order accurate Runge–Kutta scheme.

Once the boundary integral equation (11) has been solved, q_1 and q_2 are known, the velocity and the vorticity fields are readily obtained from the integral representation of the stream function (8). We get:

$$\mathbf{u}(\mathbf{x}_i^n, t^{n+1}) = \sum_k \eta\delta l_k \left(q_2^k \mathbf{rot}\mathscr{N}(\mathbf{x}_i^n - \mathbf{x}_k) - q_1^k \mathbf{rot}\frac{\partial\mathscr{N}}{\partial\mathbf{n}'}(\mathbf{x}_i^n - \mathbf{x}_k)\right) - \sum_j \Omega_j^n \mathbf{rot}\mathscr{N}(\mathbf{x}_i^n - \mathbf{x}_j^n) \tag{20}$$

and

$$\boldsymbol{\omega}(\mathbf{x}_i^n, t^{n+1}) = \sum_k \delta l_k \left(q_1^k \frac{\partial\mathscr{K}^\eta}{\partial\mathbf{n}'}(\mathbf{x}_i^n - \mathbf{x}_k) - q_2^k \mathscr{K}^\eta(\mathbf{x}_i^n - \mathbf{x}_k)\right) + \frac{1}{\eta}\sum_j \Omega_j^n \mathscr{K}^\eta(\mathbf{x}_i^n - \mathbf{x}_j^n), \tag{21}$$

where

$$\mathbf{rot}\mathscr{N}(\mathbf{x}) = \frac{1}{2\pi|\mathbf{x}|}(\mathbf{x}\times\mathbf{e}_z)\left(\frac{1}{|\mathbf{x}|} - K_1\left(\frac{|\mathbf{x}|}{\sqrt{\eta}}\right)\right), \tag{22}$$

$$\begin{aligned}\mathbf{rot}\frac{\partial\mathscr{N}}{\partial\mathbf{n}'}(\mathbf{x}) = {} & \frac{1}{2\pi|\mathbf{x}|^2}(\mathbf{x}\times\mathbf{e}_z)(\mathbf{x}\cdot\mathbf{n}')\left(-\frac{1}{|\mathbf{x}|^2} + \frac{1}{\eta}K_0\left(\frac{|\mathbf{x}|}{\sqrt{\eta}}\right) + \frac{1}{\sqrt{\eta}|\mathbf{x}|}K_1\left(\frac{|\mathbf{x}|}{\sqrt{\eta}}\right)\right) \\ & + \frac{1}{2\pi|\mathbf{x}|^2}(\mathbf{x}\times\mathbf{n}')(\mathbf{x}\cdot\mathbf{e}_z)\left(\frac{1}{|\mathbf{x}|^2} - \frac{1}{|\mathbf{x}|}K_1\left(\frac{|\mathbf{x}|}{\sqrt{\eta}}\right)\right)\end{aligned} \tag{23}$$

with K_1 the modified Bessel function of the first kind.

It is worth to notice that the velocity field (20) represents the velocity induced by the whole flow vorticity including the contribution of the perturbation at the solid wall due to the satisfaction of the no-slip condition. This equation can be viewed as the usual Biot Savart law, with both contribution coming from the discrete vorticity field and the solid boundary. The main difference is due to the Kernel $\mathscr{N}$ that includes the boundary condition for the whole domain.

The vorticity is the sum of two components. The first one is a discrete form of the boundary integral representation whereas the second is obtained by applying the PSE method [15] to the second term of this equation

$$\Omega_i^{n+1} = \Omega_i^n + \sigma_i \sum_k \delta l_k \left(q_1^k \frac{\partial \mathscr{K}^\eta}{\partial \mathbf{n}'}(\mathbf{x}_i^n - \mathbf{x}_k) - q_2^k \mathscr{K}^\eta(\mathbf{x}_i^n - \mathbf{x}_k) \right) + \sum_j \left(\Omega_j^n \sigma_i - \Omega_i^n \sigma_j \right) \mathscr{K}^\eta(\mathbf{x}_i^n - \mathbf{x}_j^n) \tag{24}$$

with σ_i the surface of the particle $\mathscr{P}_i$.

4. The inviscid flow limit

The case of small viscosity has been explored in details by Salvi [37] who was able to show that Chorin's method is the first term of an asymptotic expansion in power of η.

It is interesting to notice that a similar analysis cannot be derived for others methods [27,34]. As already mentioned, these methods are based on an actual account for the diffusion equation and the connection between the two velocity components that holds for two-dimensional flows. Therefore, they cannot be derived by the simple application of a limit process concerning the viscosity only. Beside this, these methods can be expected to have a wider application range due to a better account to the physics.

Although the complete analysis included account for the boundary curvature, a simplified presentation of the method can be obtained by considering one expansion of the Green function (7) for small η. This expansion is valid for any $|\mathbf{x}| \gg \sqrt{\eta}$ [7] so a careful analysis was conducted by Salvi in order to obtain a rigorous proof of the following result. In the limit $\sqrt{\eta} \to 0$, the K_0 function rapidly goes to zero thus yielding the first order approximation for the Green function

$$\mathscr{N}(\mathbf{x}) = \mathscr{N}_0(\mathbf{x}) + \sqrt{\eta}\mathscr{N}_1(\mathbf{x}) + \eta\mathscr{N}_2(\mathbf{x}) + \cdots = \frac{1}{2\pi}\log(\mathbf{x}) + \mathscr{O}(\sqrt{\eta}).$$

Introducing this approximation into the matrix of Eq. (12) yields

$$\mathscr{A} = \begin{bmatrix} -\frac{\partial^2 \mathscr{N}}{\partial \mathbf{n}\partial \mathbf{n}'} & \frac{\partial \mathscr{N}}{\partial \mathbf{n}} \\ -\frac{\partial \mathscr{N}}{\partial \mathbf{n}'} & \mathscr{N} \end{bmatrix} = \begin{bmatrix} -\frac{\partial^2 \mathscr{N}_0}{\partial \mathbf{n}\partial \mathbf{n}'} & \frac{\partial \mathscr{N}_0}{\partial \mathbf{n}} \\ -\frac{\partial \mathscr{N}_0}{\partial \mathbf{n}'} & \mathscr{N}_0 \end{bmatrix} + \mathscr{O}(\sqrt{\eta}). \tag{25}$$

Thanks to the expression of $\mathscr{N}_0$, we eventually obtain

$$\mathscr{A}_0 = \frac{1}{2\pi} \begin{bmatrix} -\frac{2(\mathbf{n}\cdot\mathbf{r})(\mathbf{n}'\cdot\mathbf{r})}{|\mathbf{r}|^4} + \frac{\mathbf{n}\cdot\mathbf{n}'}{|\mathbf{r}^2|} & \frac{\mathbf{n}\cdot\mathbf{r}}{|\mathbf{r}|^2} \\ \frac{\mathbf{n}'\cdot\mathbf{r}}{|\mathbf{r}|^2} & \log r \end{bmatrix}. \tag{26}$$

Introducing now this approximation into the expression of ψ_γ and its normal derivative yields the following integral representation:

$$\psi_\gamma(\mathbf{x}) = \frac{\eta}{2\pi} \int_{\partial\mathscr{D}} \left(q_2(\mathbf{x}') \log|\mathbf{x} - \mathbf{x}'| + q_1(\mathbf{x}') \frac{\mathbf{n}' \cdot (\mathbf{x} - \mathbf{x}')}{|\mathbf{x} - \mathbf{x}'|^2} \right) \mathrm{d}\mathbf{x}' \tag{27}$$

and

$$\frac{\partial \psi_\gamma}{\partial \mathbf{n}}(\mathbf{x}) = \frac{\eta}{2\pi} \int_{\partial\mathscr{D}} \left(q_2(\mathbf{x}') \frac{\mathbf{n} \cdot (\mathbf{x} - \mathbf{x}')}{|\mathbf{x} - \mathbf{x}'|^2} + q_1(\mathbf{x}') \left(\frac{\mathbf{n} \cdot \mathbf{n}'}{|\mathbf{x} - \mathbf{x}'|^2} - \frac{2(\mathbf{n} \cdot (\mathbf{x} - \mathbf{x}'))(\mathbf{n}' \cdot (\mathbf{x} - \mathbf{x}'))}{|\mathbf{x} - \mathbf{x}'|^4} \right) \right) \mathrm{d}\mathbf{x}'. \tag{28}$$

In these approximate forms, it is clear that q_1 and q_2 stand for the usual "doublet" and "source" distributions. For two-dimensional flows, it is well known that this problem does not have one unique solution unless one of these functions takes a prescribed value at a given point. However, the matricial equation can be solved iteratively by a splitting of the matrix into a diagonal part and an antisymmetric part. This technique eventually yields a method which is quite identical to Chorin's original method [11] as pointed out by Salvi [37].

5. The Stokes flow limit

In this section, the case when $\eta \to \infty$ is considered. The Green function $\mathscr{N}$ of the generalised Helmholtz problem can be expressed as an expansion of $|\mathbf{x}|/\sqrt{\eta}$ power yielding

$$\mathscr{N}(\mathbf{x}) = -\frac{1}{8\pi}(\log|\mathbf{x}| - 1)\left(\frac{|\mathbf{x}|}{\sqrt{\eta}}\right)^2 - \frac{1}{128\pi}\left(\log|\mathbf{x}| - \frac{3}{2}\right)\left(\frac{|\mathbf{x}|}{\sqrt{\eta}}\right)^4 + \frac{1}{2\pi}(\log(2) + \log(\sqrt{\eta}) - \gamma)\left(1 + \left(\frac{|\mathbf{x}|}{2\sqrt{\eta}}\right)^2 + \left(\frac{|\mathbf{x}|}{2\sqrt{2\eta}}\right)^4\right) + \mathscr{O}\left(\frac{|\mathbf{x}|}{\sqrt{\eta}}\right)^6, \tag{29}$$

where $\gamma = 0.5772156$ is the Euler constant. The previous expansion for the Green function can be rewritten

$$\mathscr{N}(\mathbf{x}) = \frac{1}{2\pi}(\log(2) - \gamma) - \frac{1}{8\pi}|\mathbf{x}|^2((\log|\mathbf{x}| - 1) - (\log(2) - \gamma))\epsilon - \frac{1}{128\pi}|\mathbf{x}|^4\left(\left(\log|\mathbf{x}| - \frac{3}{2}\right) - (\log 2 - \gamma)\right)\epsilon^2 + \mathscr{O}(\log\epsilon, \epsilon\log\epsilon, \epsilon^2\log\epsilon, \epsilon^3\log\epsilon, \epsilon^3), \tag{30}$$

where $\epsilon = 1/\eta$ is a small parameter. The first term of this expansion is a constant and does not have any incidence on the derivatives of the stream function. The second one is the Green function of the actual Stokes problem multiplied by $1/\eta$

$$\mathscr{N}_s(\mathbf{x}) = -\frac{|\mathbf{x}|^2}{8\pi}(\log|\mathbf{x}| - 1). \tag{31}$$

Introducing this form in the matrix of Eq. (12) yields for the first term of the Green function expansion for large η that is for either high viscosity or large time step

$$\mathscr{A}_0 = -\frac{1}{8\pi\eta}\begin{bmatrix} \frac{2(\mathbf{n}\cdot\mathbf{x})(\mathbf{n}'\cdot\mathbf{x})}{|\mathbf{x}|^2} + (\mathbf{n}\cdot\mathbf{n}')(2\log|\mathbf{x}| - 1) & (\mathbf{n}\cdot\mathbf{x})(2\log|\mathbf{x}| - 1) \\ (\mathbf{n}'\cdot\mathbf{x})(2\log|\mathbf{x}| - 1) & |\mathbf{x}|^2(\log|\mathbf{x}| - 1) \end{bmatrix}, \tag{32}$$

which is a $\mathscr{O}(1/(\sqrt{\eta}\log\eta))$ approximation of $\mathscr{A}$ for large η. The basic matrix of the boundary integral equation for Stokes flows can be easily recognised.

6. Numerical results

6.1. Initialisation of simulations

In order to test the proposed adaptation of the APS formulation within the framework of particle methods, we simulate the impulsively started flow around a circular cylinder at different Reynolds numbers $\mathscr{R}_e = 2U_\infty R/\nu$ with R the radius of the cylinder and U_∞ the free-stream velocity. This flow is interesting because it has been extensively studied and many suitable references are available for comparison. In a first test, our results have been compared to those of two different methods by Koumoutsakos et al. [27] and Daube [18] for a moderate Reynolds number $\mathscr{R}_e = 550$. Somewhat higher values $\mathscr{R}_e = 1000$ was used in a second test in order to verify the convergence to Chorin's original splitting which has been pointed out in Section 4. A last test concerns the case of the Stokes flow limit of Section 5 for which separate tests have also been performed for the boundary integral equation alone. In the three tests, we have computed diagnosis such as the stream function ψ, the drag coefficient C_d, the vorticity ω and the vorticity flux $\partial\omega/\partial\mathbf{n}$ at the walls. The drag coefficient was defined as

$$C_d = \frac{2}{\mathscr{R}_e}\int_0^{2\pi}\left(\omega - \frac{\partial\omega}{\partial\mathbf{n}}\right)\tau_x\,d\theta. \tag{33}$$

Because of the impulsively started flow, a specific initialisation procedure had to be used. The method introduced by Koumoutsakos et al. was used. At time $t = 0^-$, particles were created around the cylinder on a crown with thickness proportional to $\sqrt{2\delta t/\mathscr{R}_e}$.

This crown was discretised with M_r particles layers. In our calculations, M_r was always equal to 20. The total number of particles used for the crown discretisation is $M_r \times M$ where M is the number of segments $\mathscr{S}_k$ used in the resolution of the boundary integral equation (see Fig. 1). This number was selected according to the results of a refinement study conducted for different Reynolds number values (see Fig. 2 for an example with $\mathscr{R}_e = 550$). The values of the other numerical parameters used have been gathered in Table 1.

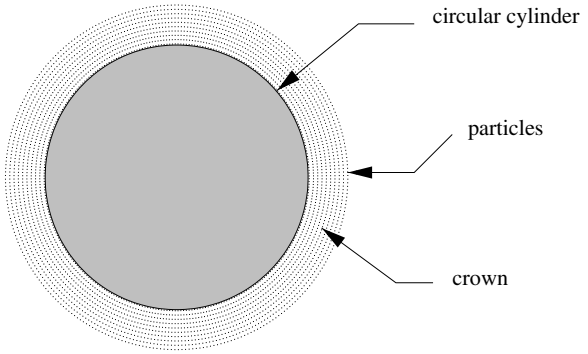

Fig. 1. Example of a crown around the circular cylinder for the initialisation of particles.

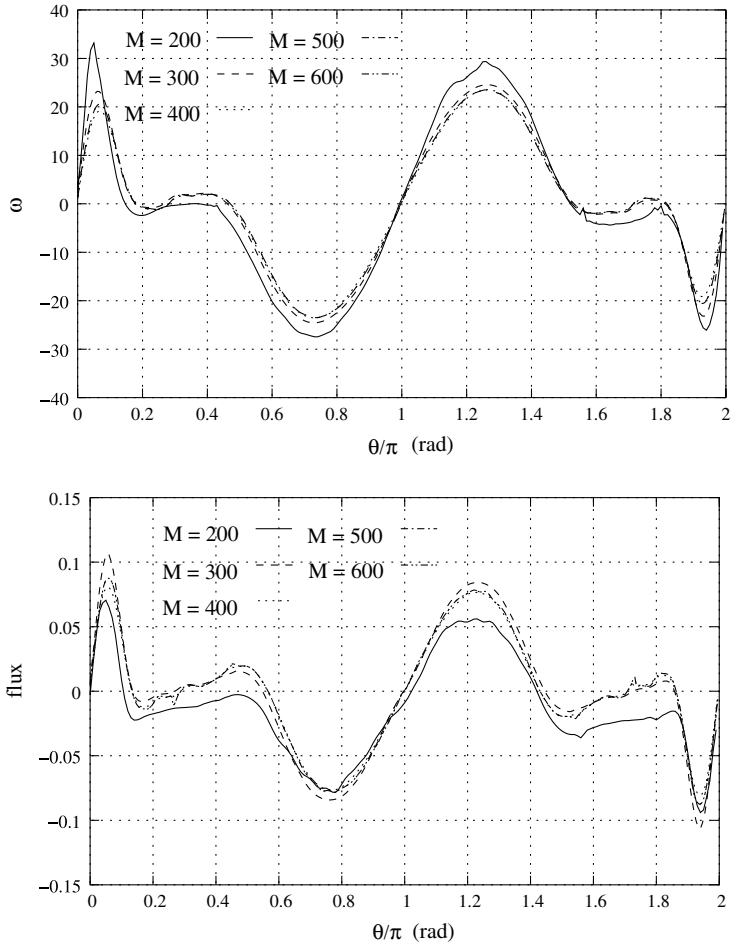

Fig. 2. Evolution with numerical parameter M of the vorticity ω (top) and the vorticity flux $\partial\omega/\partial\mathbf{n}$ (bottom) on the surface of the cylinder $\partial\mathscr{D}$ for $\mathscr{R}_e = 550$ from the present method.

At this stage, these particles had no vorticity. The no-slip condition at the solid walls was not satisfied and this initial flow has to be corrected. This correction was obtained through the distribution of the vorticity flux onto the surrounding particles which initial weight was taken as

Table 1
Numerical parameters used for the simulations

$\mathscr{R}_e$	δt	η	$\mathscr{N}_f$	M	M_r	$N_{initial}$	N_{final}	σ_{mini}	σ_{max}
1000	0.05	0.0001	4	1000	20	2×10^4	119,472	2.6×10^{-5}	7.4×10^{-5}
550	0.05	0.00018	4	500	20	10^4	53,748	6.8×10^{-5}	2.2×10^{-4}
100	0.05	0.001	4	400	20	8×10^3	36,501	2.0×10^{-4}	1.2×10^{-3}
60	0.05	0.0017	4	400	20	8×10^3	36,363	2.6×10^{-4}	1.7×10^{-3}
40	0.05	0.0025	4	400	20	8×10^3	35,941	3.2×10^{-4}	2.2×10^{-3}
20	0.05	0.005	4	400	20	8×10^3	38,704	4.5×10^{-4}	4.0×10^{-3}
10	0.05	0.01	4	400	20	8×10^3	38,956	6.4×10^{-4}	6.5×10^{-3}
5	0.05	0.02	4	400	20	8×10^3	39,892	9.1×10^{-4}	1.1×10^{-3}
2	0.05	0.05	4	400	20	8×10^3	39,880	1.5×10^{-3}	2.8×10^{-2}
1	0.05	0.1	4	400	20	8×10^3	38,144	2.1×10^{-3}	3.5×10^{-2}
0.1	0.05	1	4	400	20	8×10^3	37,055	1.5×10^{-2}	7.9×10^{-1}
0.01	0.05	10	4	400	20	8×10^3	35,378	3.2×10^{-2}	2.2
0.001	0.05	100	4	400	20	8×10^3	35,572	1.9×10^{-1}	22
0.0001	0.05	1000	4	400	20	8×10^3	48,408	1.45	3.0×10^2

$$\Omega_i^0 = \sigma_i \sum_k \frac{\gamma_k}{1-\sqrt{2\pi\delta t/\mathscr{R}_e}}(A_k+B_k)\frac{1}{\sqrt{8\delta t/\mathscr{R}_e}}\exp\left(\frac{-\delta x^2}{8\delta t/\mathscr{R}_e}\right) \tag{34}$$

with

$$A_k = \operatorname{erf}\left(\frac{\delta y+\delta l_k/2}{\sqrt{8/\mathscr{R}_e\delta t}}\right), \tag{35}$$

$$B_k = \operatorname{erf}\left(\frac{\delta l_k/2-\delta y}{\sqrt{8/\mathscr{R}_e\delta t}}\right), \tag{36}$$

$$\delta x = (x_i-x_k)\tau_{xk}+(y_i-y_k)\tau_{y_k}, \tag{37}$$

$$\delta y = (x_i-x_k)\tau_{y_k}+(y_i-y_k)\tau_{xk}, \tag{38}$$

where τ_{xk} and τ_{yk} are the components of the unit clockwise oriented tangent $\boldsymbol{\tau}_k$ to the cylinder section at point $\mathbf{x}_k$, that is a vector parallel to the segment $\mathscr{S}_k$. The strength γ_k is given by

$$\gamma_k = -\mathbf{e}_x\cdot\boldsymbol{\tau}_k. \tag{39}$$

In particle methods, an overlapping condition must be satisfied to ensure the accuracy of the numerical simulations. Because of Lagrangian distortion induced by the flow, a re-griding procedure is then necessary. In this work, the re-griding procedure introduced by Jollès and Huberson [23] was used.

6.2. Moderate Reynolds numbers

In this first test, the results of the particle method with the APS formulation have been compared to those of Koumoutsakos et al. and Daube's methods.

These two methods were selected because the first one is a reference vortex method whereas the second is a finite differences method using the matrix influence method. A Reynolds number $\mathscr{R}_e = 550$ was selected. It corresponds to moderate Reynolds numbers for which the direct inversion of matrix $\mathscr{A}$ of Eq. (12) is possible. The simulation was performed up to an adimensional time $t = U_\infty T/R = 7$ with a time step $\delta t = 0.05$. A re-griding frequency $N_f = 4$ was selected. The number M of segments $\mathscr{S}_k$ was fixed to 500.

In Figs. 3 and 4, the vorticity ω obtained with the present method and Daube's method has been plotted at different times. Very similar solutions were obtained with the two methods although the iso-line are somewhat smoother with the last one. This can be attributed to the larger viscous diffusion necessary to ensure the stability of finite difference methods. Moreover, the boundary conditions are not simultaneously solved in this method which was essentially design to derive proper boundary conditions for the vorticity.

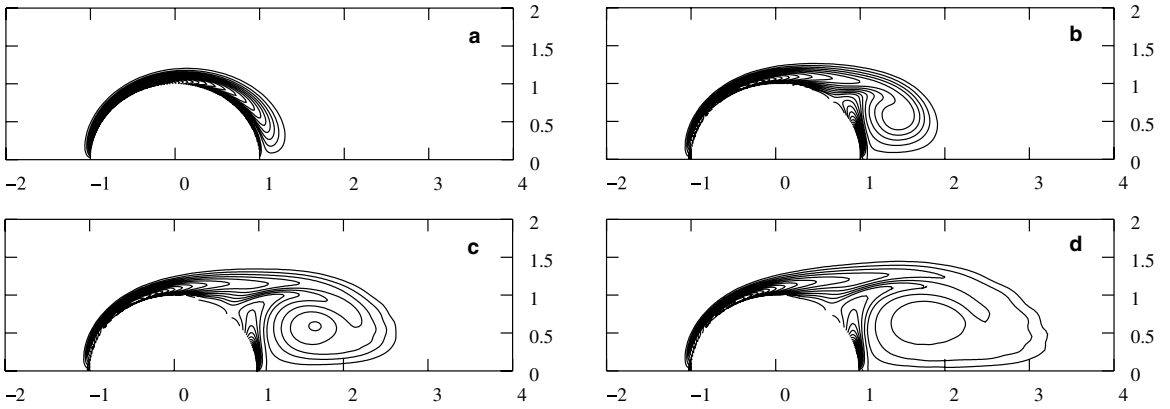

Fig. 3. Vorticity field ω for an impulsively started circular cylinder obtained with the present method for $\mathscr{R}_e = 550$ and different times $t = 1$ (a), $t = 3$ (b), $t = 5$ (c) and $t = 7$ (d). The levels are by steps of 4.

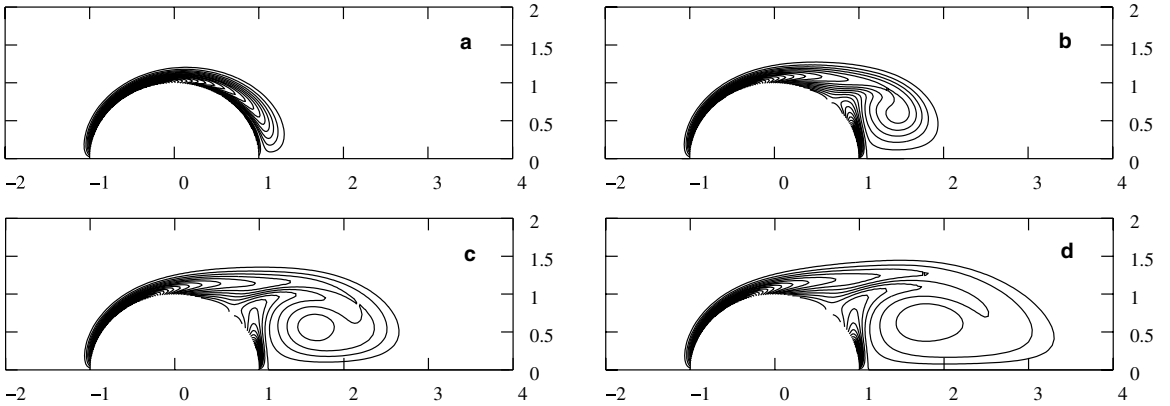

Fig. 4. Vorticity field ω for an impulsively started circular cylinder obtained with Daube's method for $\mathscr{R}_e = 550$ and different times $t = 1$ (a), $t = 3$ (b), $t = 5$ (c) and $t = 7$ (d). The levels are by steps of 4.

The onset of a symmetrical recirculating zone attached to the cylinder in which a main and a secondary eddies develop was obtained with the convenient respective diameters. Fig. 5 shows the time evolution of the drag coefficient C_d for the present method and Koumoutsakos et al. method and we can observe that the two methods give almost the same time evolution.

In this simulation, the final number of particles was 54,000 and the particles surfaces σ_i range from 6.8×10^{-5} to 2.2×10^{-4} (see Table 1).

In Fig. 6, the vorticity ω and the vorticity flux $\partial\omega/\partial\mathbf{n}$ on the surface of the cylinder $\partial\mathscr{D}$ have been reported for both methods. For these two quantities, the present method gives values slightly lower than those obtained by Koumoutsakos et al. As already mentioned, this is the most probable cause for the discrepancy observed on the drag coefficient.

This point has been further examined for the early stage of the impulsively started flows for $Re = 200$, for which case an analytical solution exists [13]. The results obtained were also compared to that of Koumoutsakos (see Fig. 7). It was observed that, for suitable discretisation parameters ($M > 600$) the two numerical methods gave almost the same results, both being slightly higher than the analytical solution. Also, we can verified that the friction and pressure drags are equally important at the beginning of the motion.

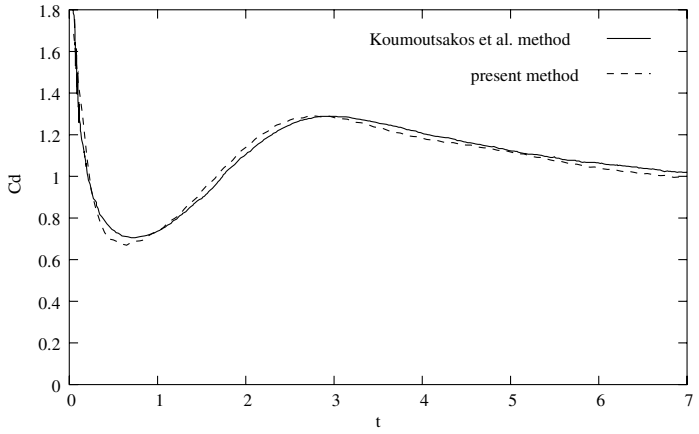

Fig. 5. Evolution with time of the drag coefficient C_d for an impulsively started circular cylinder at $\mathscr{R}_e = 550$ from the present method (discontinuous line) and Koumoutsakos et al. method (solid line).

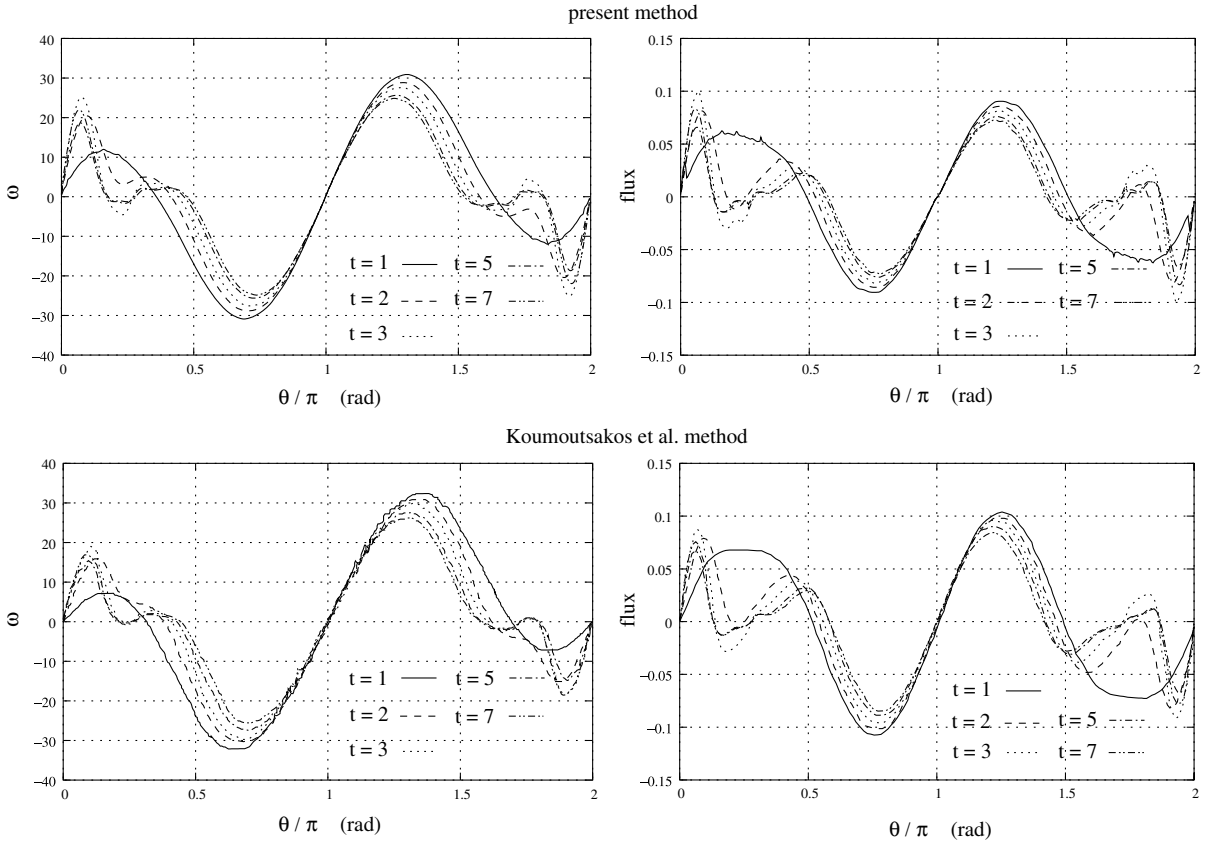

Fig. 6. Evolution with time of the vorticity ω (left) and the vorticity flux $\partial\omega/\partial\mathbf{n}$ (right) on the surface of the cylinder $\partial\mathscr{D}$ for $\mathscr{R}_e = 550$ from the present method (top) and Koumoutsakos et al. method (bottom).

6.3. Higher Reynolds numbers

In these tests, the results of the present method have been first compared to those of Chorin's first method for the case of vanishing or, at least, weak viscosity. A Reynolds number $\mathscr{R}_e = 1000$ was selected first. Two

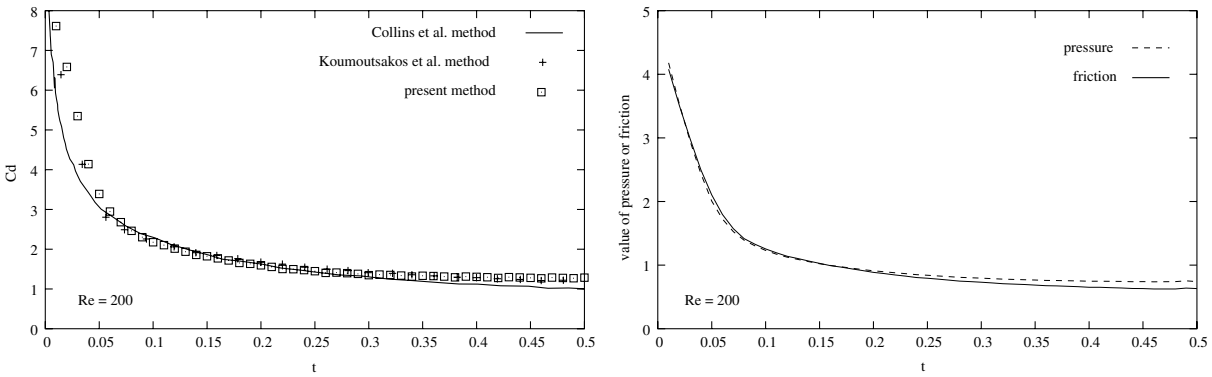

Fig. 7. Comparison of the drag coefficient C_d of an impulsively started circular cylinder for $\mathscr{R}_e = 200$, from the present method (top), Koumoutsakos et al. method (bottom) and theoretical predictions from Collins et al. (left). In the right figure, evolution with time of the form and friction drag coefficient.

numerical simulations have been performed, one with the initial APS formulation and the other with the asymptotic formulation of Section 4. As in the previous test, both methods were compared to Koumoutsakos et al. and Daube's methods. The simulations were performed up to an adimensional time $t = 7$ with a time step

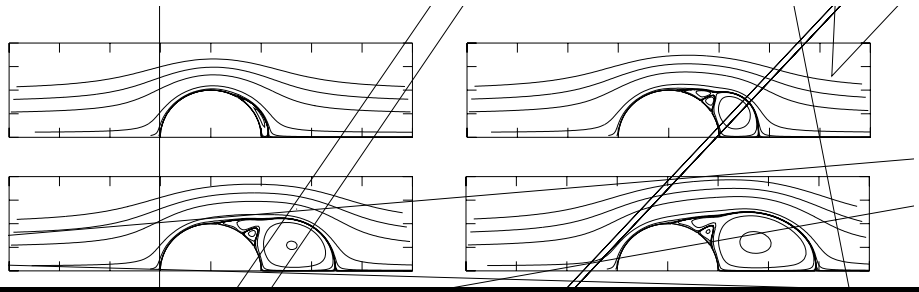

$\delta t = 0.05$. The re-griding frequency N_f remains unchanged. The number M of segments $\mathscr{S}_k$ was fixed to 1000. Fig. 8 shows the stream function ψ at different times $t = 1$, 3, 5 and 7 after the impulsive start for the present method with the initial APS formulation or the asymptotic APS formulation and Daube's method. We can observe that very similar results were obtained with the two APS formulations, both being close to Daube's results. In Fig. 9, the history of the drag coefficient C_d obtained with the present method equipped with the initial and asymptotic APS formulation have been plotted together with Koumoutsakos et al. method. The present results are in very good agreement with those of Koumoutsakos et al. for both cases.

Although it would be more comfortable and of great interest to know where the "exact" solution lies, it is just possible to point out that the different solutions were obtained with different methods. Consequently, they probably lie within the expected accuracy range of these methods. At time $t = 5$, the drag coefficient C_d was found to be about 1.098 with the asymptotic APS formulation, 1.121 with the initial APS formulation and 1.097 with Koumoutsakos et al. method that is with a less than 0.1% gap between the first and the last methods which can be considered has the best possible choice at this Reynolds number. These results are also consistent with the asymptotic analysis which validity is limited to the higher Reynolds numbers.

The vorticity ω and the vorticity flux $\partial\omega/\partial\mathbf{n}$ on the surface of the cylinder $\partial\mathscr{D}$ have also been reported for the two APS formulations and Koumoutsakos et al. method in Fig. 10.

6.4. Low Reynolds numbers

The aim of this section is the study of the convergence of the present method for the case of increasing viscosity. This has been achieved by considering flows with Reynolds numbers $\mathscr{R}_e$ ranging from 0.0001 to 100. The calculations have been performed up to an adimensional time $t = 7$ with a time step $\delta t = 0.05$. The re-griding frequency N_f remains unchanged. For all these simulations, the number M of segments $\mathscr{S}_k$ was set to 400.

First, the values of the drag coefficients obtained with the initial APS formulations and the asymptotic approximation of Section 5 were reported in Table 2.

The reference solution was provided by two analytical curves for the drag coefficient. The first one for $\mathscr{R}_e < 0.01$ is the well-known lamb solution [3]. For higher $\mathscr{R}_e$, an empirical law obtained through an identification procedure based on experimental data by Chaplin [9] was used. It can be observed that the results of the asymptotic formulation are closer to these references for Reynolds numbers up to 0.1.

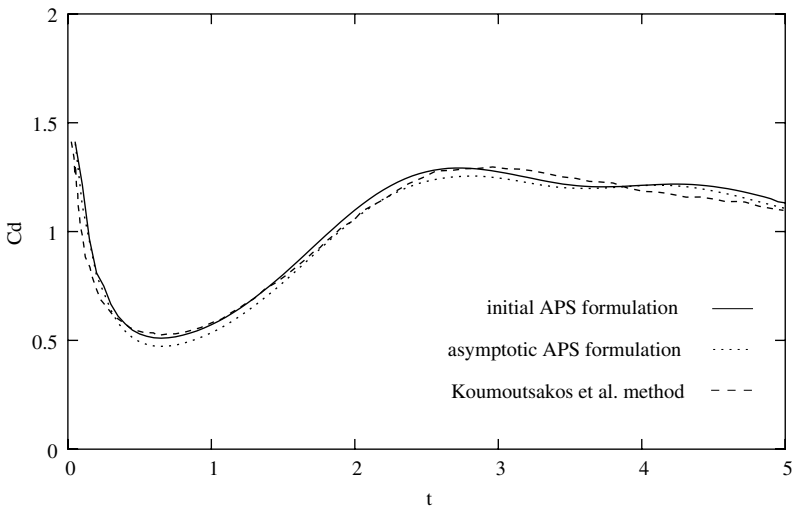

Fig. 9. Evolution with time of the drag coefficient C_d for an impulsively started circular cylinder at $\mathscr{R}_e = 1000$ from the present method with the initial APS formulation (solid line) or the asymptotic APS formulation (dotted line) and Koumoutsakos et al. method (discontinuous line).

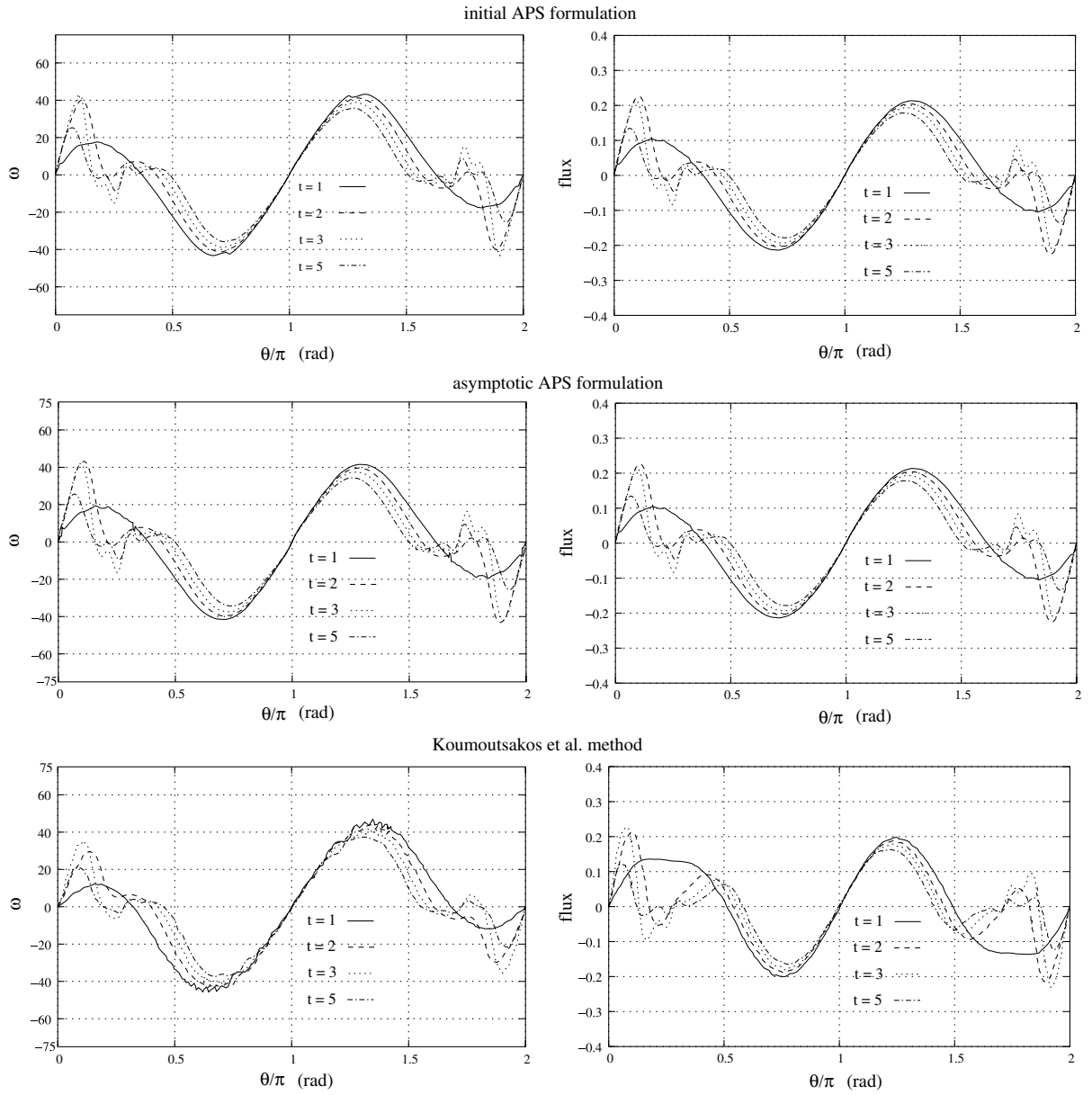

Fig. 10. Evolution with time of the vorticity ω (left) and the vorticity flux $\partial\omega/\partial\mathbf{n}$ (right) on the surface of the cylinder $\partial\mathscr{D}$ for $\mathscr{R}_e = 1000$ from the present method with the initial APS formulation (top) or the asymptotic APS formulation (middle) and Koumoutsakos et al. method (bottom).

Table 2
Comparison of the drag coefficient C_d with the initial and asymptotic APS formulations

$\mathscr{R}_e$	η	Analytical solution	Asymptotic APS formulation	Initial APS formulation
1	0.1	10.32	No simulation	9.91 (3.92%)
0.1	1	56.12	No simulation	58.43 (4.11%)
0.01	10	3.810×10^2	3.696×10^2 (3%)	3.375×10^2 (11.43%)
0.001	100	2.821×10^3	2.644×10^3 (6.26%)	2.468×10^3 (12.5%)
0.0001	1000	2.242×10^4	2.140×10^4 (4.5%)	1.956×10^4 (12.76%)

It can be attributed to the fact that the asymptotic formulation numerically solve the equation actually used to derive the analytical solution. The difference between the asymptotic and full APS solutions is, therefore, a measure of the asymptotic error made when substituting Stokes to Navier–Stokes equations for low Reynolds numbers.

It is well known that the Stokes solution is the inner solution of a singular perturbation problem. As a result, the asymptotic APS formulation which is based on an actual flow solver may be much closer to the usual matched asymptotic expansion solution whereas the full APS formulation can be seen as a numerical approximation of a uniformly valid solution. Beside this, it must be kept in mind that the difference between the two methods is a numerical error rather than an exact measure of the difference between two analytical solutions.

For higher Reynolds number, the initial APS formulation provides a better approximation.

For $\delta t = 0.05$ and $\mathscr{R}_e = 0.1$, η is equal to 1 and can no longer be considered as a small parameter. This upper limit was further tested by trying different combinations for the time step and the Reynolds number giving the same value for η. The previous conclusion was confirmed by these calculations.

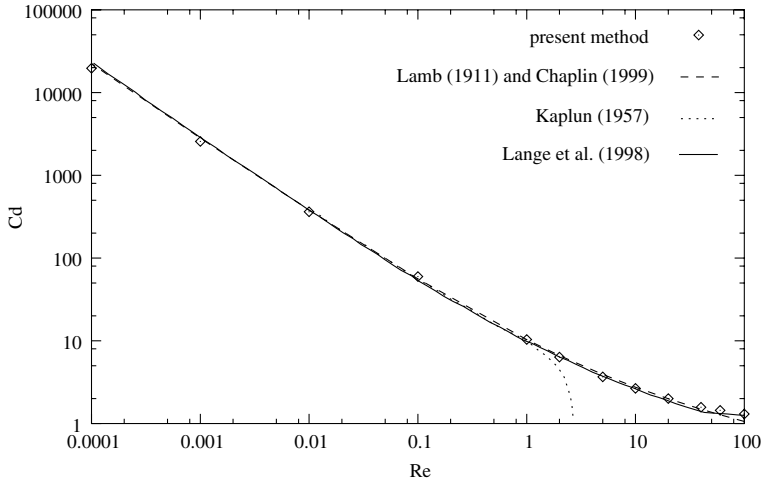

Fig. 11. Comparison of the drag coefficient C_d with theoretical and numerical results: dotted line is analytical solutions given by Lamb (in [9]) and Chaplin [9] – dashed line is results of matched asymptotic expansion given by Kaplun [26] – solid line is numerical results given by Lange et al. [28] – lozenges are numerical results given by the present method.

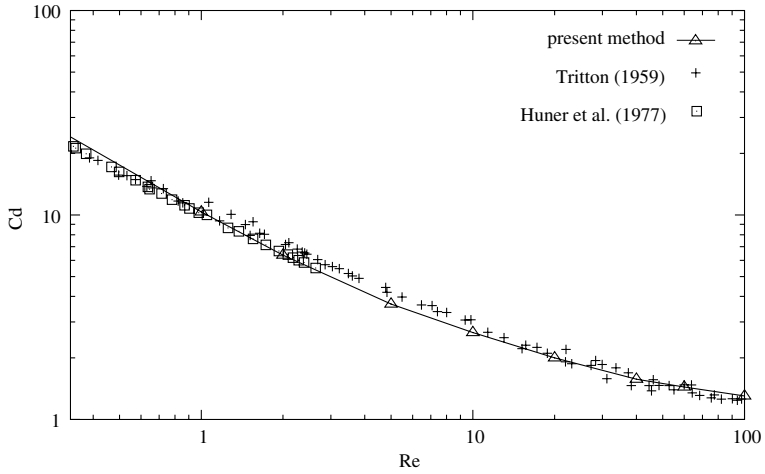

Fig. 12. Comparison of the drag coefficient C_d with numerical and experimental results: cross and squares are experimental results given by Tritton [38] and Huner et al. [25] – solid line is numerical results given by the present method.

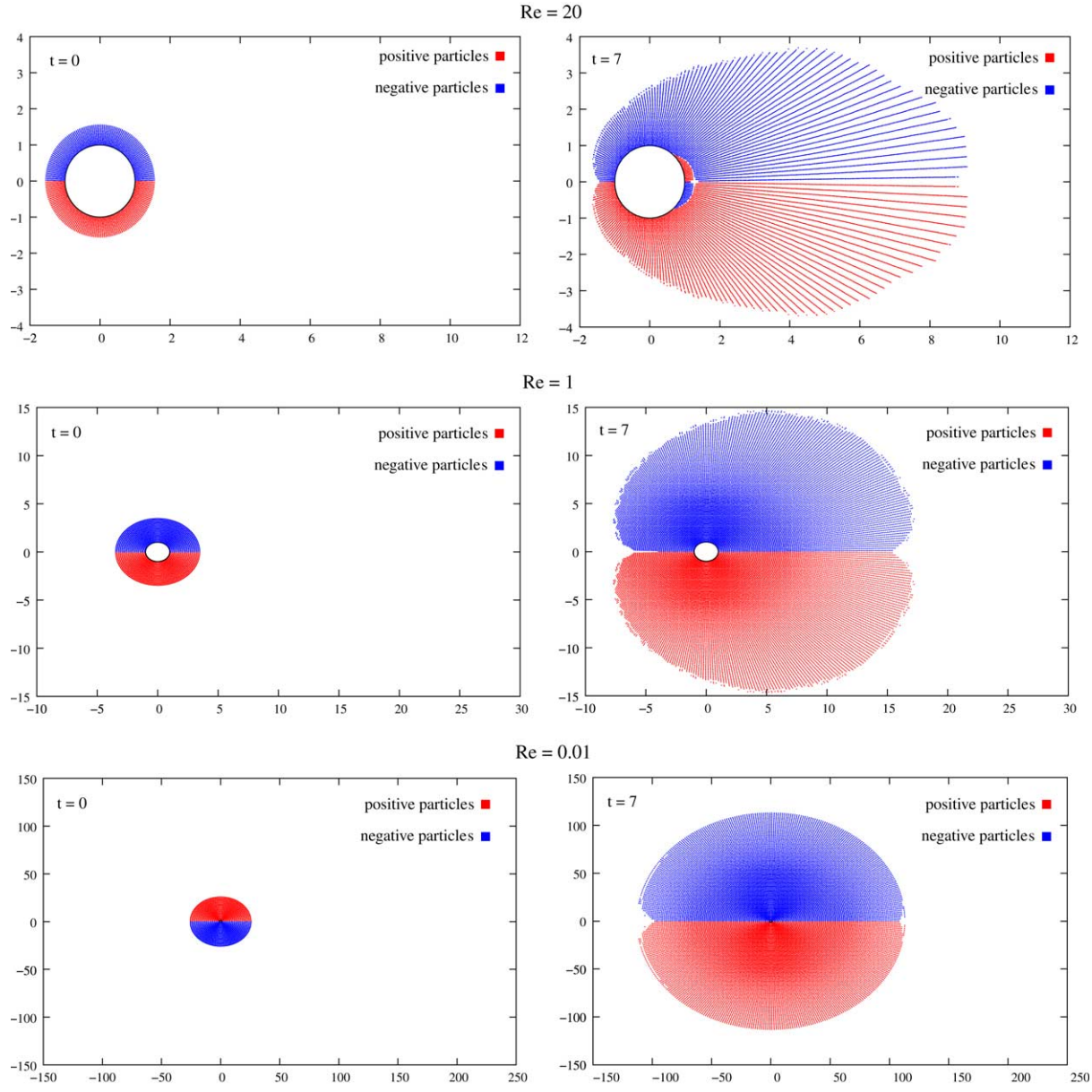

Fig. 14. Particles location for three different low Reynolds number $\mathscr{R}_e = 0.01,\ 1$ and 20 at $t = 0$ and 7.

A particular aspect in these calculations is the particle location. For the lower Reynolds, the vorticity is mainly diffused which means that the vorticity can reached relatively high values in the far field. Therefore, a large number of particle was used, not only within the wake but also upstream where diffusion effects dominate the convective effects. This is illustrated in Fig. 14 where the final particle locations have been reported for three different Reynolds numbers.

An other important question concerning these low Reynolds number flows has been addressed. Two asymptotic formulations have been derived from the APS formulation. The behaviour of these different formulation regarding the Stokes flow approximation was also investigated. The results have been reported in Fig. 15. It was observed that the convergence of the low Reynolds approximation is always faster than that of the complete formulation and that the high Reynolds formulation converge to a slightly different value

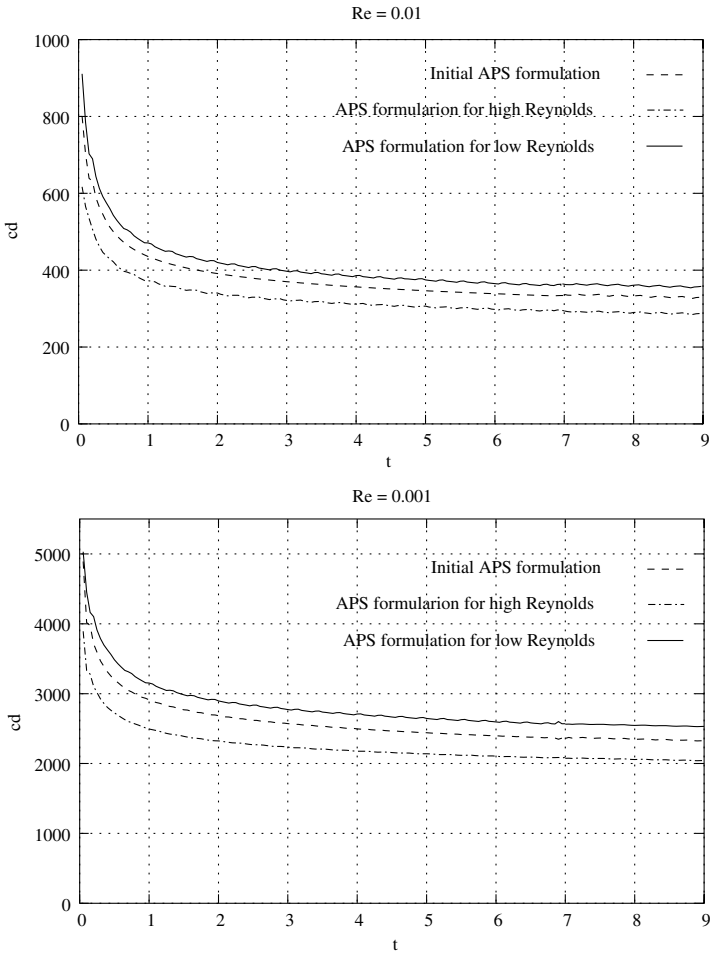

Fig. 15. Time history of the drag coefficient for the three APS formulations and two Reynolds number $\mathscr{R}_e = 0.01$ and $\mathscr{R}_e = 0.001$.

for the lower Reynolds. This can be attributed to the structure of the numerical algorithm which always necessitates a transfer of the vorticity onto the moving particles, even in the present case where diffusion alone represents more than 99% of the vorticity transfer.

7. Conclusions

An algorithm originally derived by Achdou, Pironneau and further developed by Salvi [1,2,37] was adapted to particle methods in order to improve the treatment of boundary conditions for low Reynolds number flows. Two asymptotic formulations were also derived and implemented for the extreme cases of high and low Reynolds numbers.

It was found that the method is almost as good as the best methods known up today while it still works for very low Reynolds number as well. This last conclusion was supported by extensive comparisons with results from various publications.

The high Reynolds approximation of the APS was found to be very similar to Chorin's method by Salvi. Applied within the same particle method framework to the same problem, it was found to provide results very close to that of our reference particle method, even closer than that obtained by the original APS formulation. The possibility to consider this method as the first term of an asymptotic expansion could provide a guide for any improvement by computing the second or third order terms.

Our last conclusion concerns the low Reynolds approximation. It has been demonstrated that the Stokes integral solution can be substituted to the APS formulation in this case. As a result, low Reynolds number flows including non negligible inertia effects can be simulated as a perturbation of a Stokes flow. Moreover, a three-dimensional extension of the method can be easily derived thanks to the well developed theory of boundary integral equation for three-dimensional Stokes flows.

References

[1] Y. Achdou, O. Pironneau, Integral equations for the generalized Stokes operator, CR Acad. Sci. Paris t. 415 (Série I) (1992) 91–96.
[2] Y. Achdou, O. Pironneau, A fast solver for Navier–Stokes equations in the laminar regime using mortar finite element and boundary element methods, SIAM J. Numer. Anal. 32 (4) (1993) 985–1016.
[3] G.K. Batchelor, An Introduction to Fluid Dynamics, Cambridge University Press, Cambridge, 1967.
[4] J.T. Beale, A convergent 3D vortex methods with grid free stretching, Math. Comput. 46 (1986) 401–424.
[5] J.T. Beale, A. Majda, Rates of convergence for viscous splitting of the Navier Stokes equations, Math. Comput. 37 (1981) 243–259.
[6] R. Bouard, M. Coutanceau, The early stage of development of the wake behind an impulsively started cylinder for $40 < Re < 10^4$, J. Fluid Mech. 101 (1980) 583–607.
[7] F. Bowman, Introduction to Bessel Functions, Dover, New York, 1958.
[8] B.L. Buzbee, F.W. Dorr, The direct solution of the biharmonic equation on rectangular regions and the Poisson equation on irregular regions, SIAM J. Numer. Anal. 11 (1974) 753–763.
[9] J.R. Chaplin, History forces and the unsteady wake of a cylinder, J. Fluid Mech. 393 (1999) 99–121.
[10] J.P. Choquin, S. Huberson, Particles simulation of viscous flow, Comput. Fluids 17 (1989) 397–410.
[11] A.J. Chorin, Numerical study of slightly viscous flow, J. Fluid Mech. 57 (1973) 785–796.
[12] A.J. Chorin, Vortex sheet approximation of boundary layers, J. Comput. Phys. 27 (1978) 428–442.
[13] W.M. Collins, S.C.R. Dennis, The initial flow past an impulsively started circular cylinder, Quart. J. Mech. Appl. Math. XXVI (Pt. 1) (1973) 53–75.
[14] G.H. Cottet, A new approach for the analysis of vortex methods in two and three dimensions, Ann. Inst. H. Poincaré 5 (1988) 227–285.
[15] G.H. Cottet, P. Koumoutsakos, Vortex Methods Theory and Practice, Cambridge University Press, Cambridge, 2000.
[16] G.H. Cottet, S. Mas-Gallic, A particle method to solve the Navier–Stokes system, Numer. Math. 57 (1989) 805.
[17] G.H. Cottet, P. Poncet, Advances in direct numerical simulations of 3D wall-bounded flows by vortex-in-cell methods, J. Comput. Phys. 193 (2003) 136–158.
[18] O. Daube, Resolution of the 2D Navier–Stokes equations in velocity–vorticity form by means of an influence matrix technique, J. Comput. Phys. 103 (1992) 402–414.
[19] P. Degond, S. Mas-Gallic, The weighted particle method for convection-diffusion equations, Part 2: the anisotropic case, Math. Comp. 53 (1989) 509.
[20] J.D. Eldredge, A. Leonard, T. Colonius, A general treatment of derivatives in particle methods, J. Comput. Phys. 180 (2002) 686–709.
[21] A. Gharakhani, A.F. Ghoniem, in: 3D Vortex Simulation of Flow in An Opposed-Piston Engine, Vortex Flows and Related Numerical Methods III ESAIM: Proceedings, vol. 7, 1999, pp. 161–172.
[22] J.M.R. Graham, Computation of viscous separated flow using particle method, in: K.W. Morton (Ed.), Numerical Methods in Fluid Mechanics, vol. 3, Oxford University Press, Oxford, 1988, pp. 310–317.
[23] S. Huberson, A. Jollès, Correction de l'erreur de projection dans les méthodes particles/maillage, Rech. Aérosp. 4 (1990) 1–6.
[24] S. Huberson, A. Jollès, W. Shen, Numerical simulation of incompressible viscous flows by means of particle methods, Lect. Appl. Math. Ser. 28 (1991) 369–384.
[25] B. Huner, R.G. Hussey, Cylinder drag at low Reynolds number, Phys. Fluids 20 (8) (1977) 1211–1218.
[26] S. Kaplun, Low Reynolds number flow past a circular cylinder, J. Math. Mech. 6 (1957) 595–603.
[27] P. Koumoutsakos, A. Leonard, High resolution simulations of the flow around an impulsively started cylinder using vortex methods, J. Fluid Mech. 296 (1995) 1–38.
[28] C.F. Lange, F. Durst, M. Breuer, Momentum and heat transfer from cylinders in laminar crossflow at $10^{-4} \leqslant Re \leqslant 200$, Int. J. Heat Mass Transf. 41 (1998) 3409–3430.
[29] S.H. Leel, L.G. Leal, Low Reynolds number flow past cylindrical bodies of arbitrary cross sectional shape, J. Fluid Mech. 164 (1986) 401–427.
[30] A. Leonard, Computing three-dimensional incompressible flows with vortex elements, Annu. Rev. Fluid Mech. 17 (1985) 523.
[31] E.D. Martin, A generalized capacity matrix technique for computing aerodynamic flows, Comput. Fluids 2 (1974) 79.
[32] S. Mas-Gallic, Deterministic particle method: diffusion and boundary conditions, Lect. Appl. Math. Ser. 28 (1991) 433–465.
[33] M. Napolitano, G. Pascazio, L. Quartapelle, A review of vorticity conditions in the numerical solution of the equations, Comp. Fluids 28 (1999) 139–185.
[34] P. Ploumhans, G.S. Winckelmans, Vortex methods for high-resolution simulations of viscous flow past bluff bodies of general geometry, J. Comput. Phys. 165 (2000) 354–406.
[35] P. Ploumhans, G.S. Winckelmans, J.K. Salmon, A. Leonard, M.S. Warren, Vortex methods for direct numerical simulation of three-dimensional bluff body flows: application to the sphere at $Re = 300$, 500 and 1000, J. Comput. Phys. 178 (2002) 427–463.

[36] I. Proudman, J.R. Pearson, Expansions at small Reynolds numbers for the flow past a sphere and a circular cylinder, J. Fluid Mech. 2 (1957) 237–262.
[37] J. Salvi, Contribution théorique et numérique des méthodes intégrales de frontière à la résolution des équations de Navier Stokes bidimensionnelles en formulation vitesse tourbillon, Ph.D. Thesis, Ecole polytechnique, 1999.
[38] D.J. Tritton, Experiments on the flow past a circular cylinder at low Reynolds numbers, J. Fluid Mech. 6 (1959) 547–567.